Surfaces and Interfaces 20 (2020) 100579

Contents lists available at ScienceDirect

Surfaces and Interfaces

journal homepage: www.elsevier.com/locate/surfin

Effects of lattice mismatches in In_2O_3/substrate structures on the structural, morphological and electrical properties of In_2O_3 films

A. Bouhdjer[a,b,*], H. Saidi[b], A. Attaf[b], A. Yahia[b], M.S. Aida[c], O. Benkhetta[b], L. Bouhdjer[d]

[a] Département socle commun sciences et technologie, faculté de technologie, université Batna 2, N3, Batna, Algeria
[b] Physic Laboratory of Thin Films and Applications LPCMA, University of Biskra, Algeria
[c] Center of Nanotechnology King, Abdulaziz University, Jedahh, Saudi Arabia
[d] Laboratory of Crystallography, Department of Physics, Mentouri University of Constantine, Constantine 25000, Algeria

ARTICLE INFO

Keywords:
Indium oxide
Lattice mismatch
Ultrasonic spray
Structural and electrical properties

ABSTRACT

Indium oxide thin films were deposited by ultrasonic spray technique on ITO coated glass and single crystalline Si (400) substrates at 400 °C. Lattice mismatch effect on the crystalline structure, surface morphology and electrical properties of these samples is then studied. X-ray diffraction (XRD) and Raman spectroscopy patterns suggest that the films deposited on ITO coated glass substrate are polycrystalline in nature having a cubic crystal structure with a preferred grain orientation along the (222) plane. However, films deposited on Si wafer substrate, exhibit randomly oriented growth. The crystallite size varies from 18 to 66.5 nm. AFM topographical images revealed that the In_2O_3/ITO films follow 2D or layer-by-layer-growth. But in the case of In_2O_3/Si films, 3D or island growth becomes dominant. The In_2O_3/ITO films is found to exhibit a higher value of conductivity ($\sigma = 5 \times 10^2\ \Omega^{-1}\ cm^{-1}$) than the In_2O_3/Si films, and the low value of the RMS roughness (9.83 nm).

1. Introduction

Quite recently, considerable attention has been paid to the transparent conducting oxides (TCO) thin films due to their interesting physical properties, which combine electrical conduction and optical transparency in the visible spectral range of UV–Vis. Among the TCO is indium oxide (In_2O_3), which is a n-type semiconductor, It is a wide band-gap semiconductor and has a band gap of 3.5–3.75 eV, dielectric constant of 8.9 and a cubic (Ia3) structure of lattice constant 1.0117 nm, for this it is considered the most important transparent conducting oxide for various scientific technologies such as solar cell, gas sensors, and liquid crystal displays (LCD) [1]. The In_2O_3 thin films have been prepared on a variety of substrates by different methods, such as: vacuum evaporation [2], direct-current (dc) magnetron sputtering and radio-frequency (rf) magnetron sputtering [3,4], spray pyrolysis [5], molecular beam epitaxy [6] and sol–gel method [7]. In this work, we will focus on the spray ultrasonic technique to deposit In_2O_3 thin films.

In order to obtain the fundamental knowledge about the growth mechanism of In_2O_3 thin layers deposited by this technique, we have already studied the effect of several parameters on the properties of In_2O_3 thin layers, such as: deposition time [8], annealing temperature [9], Solution flow rate [10] and the nature of the substrate [11]. Depending on the results of these studies, we found that the structural and electrical properties of In_2O_3 thin layers strongly depend on the nature of the substrate. The preferred growth orientation changed from the (222) to (400) plan for the films deposited on the Kcl single crystal substrate [11]. L. Álvarez-Fraga et al. [12] and Neeti Tripathi et al. [13] also found that properties of indium oxide depend to the nature of the substrate. Until now, to the best of our knowledge, few studies report the influence of lattice mismatch on the properties of In_2O_3 thin films deposited by spray ultrasonic technique. In this context, we recommend to investigate the relationship between lattice mismatch and the structural, morphological and electrical properties of In_2O_3 thin films. In order to achieve this goal, indium oxide thin films are deposited on ITO coated glass (labeled In_2O_3/ITO films) and single crystalline Si (400) (labeled In_2O_3/Si films) substrate.

2. Experimental procedure

In the present work, Indium oxide thin layers were deposited on ITO coated glass (conducting glass) and single crystal Si (400) substrates with dimension of ~25 × 15 mm^2 at 450 °C, using the ultrasonic spray technique (See the Fig. 1). The starting solution was prepared by dissolving indium chloride $InCl_3$ (powder, Merk, 99.9 Sigma-Aldrich) in an appropriate amount of ethanol C_2H_5OH (96% VWR chemicals

* Corresponding author.
E-mail address: a.bouhdjer@univ-batna2.dz (A. Bouhdjer).

https://doi.org/10.1016/j.surfin.2020.100579
Received 3 March 2020; Received in revised form 7 May 2020; Accepted 9 June 2020
Available online 10 June 2020

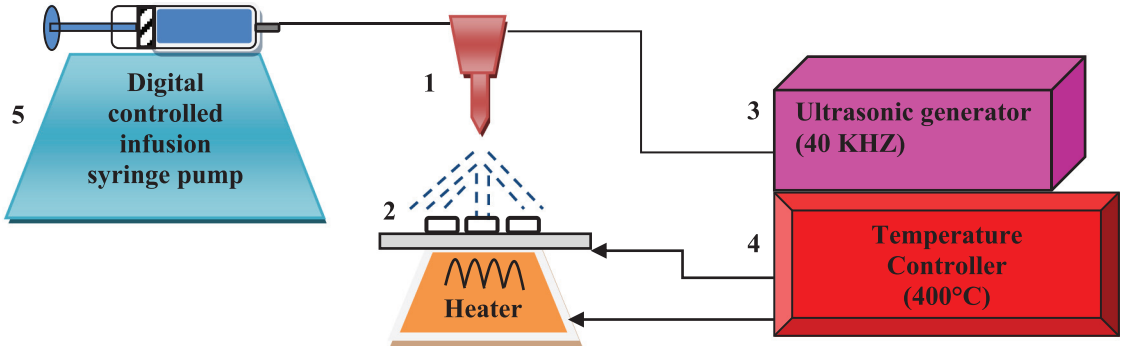

1- Spray nozzle, 2- Substrate,3- Ultrasonic generator,4- Thermocouple. 5- Syringe (container of solution).

Fig. 1. Schematic diagram of the ultrasonic spray technique.

Table 1
Deposition parameters used to elaborate the In_2O_3 thin films by spray ultrasonics.

Deposition time (min)	Solution flow rate (ml/h)	Temperature (°C)	Distance spray nozzle–substrate (cm)	Solution concentration (mol/l)
4	40	400	5.5	0.1

(France)). Using the Syringe pump PHOENIX D-CP, the chemical solution arrives to the ultrasonic atomizer which fractionates it to micro droplets that fall on the heated substrate. We changed the substrate, and we fixed the others deposition parameters, such as: the solution concentration, the distance nozzle-substrate, Solution flow rate and the deposition time. The experimental conditions are summarized in the Table 1.

These deposited films were characterized by an X-ray diffractometer (X'PERT PRO) with Cu-Kα radiation (λ = 1.5418 Å) and a (Jobin–Yvon) μ-Raman spectrometer at room temperature (RT) to define the structural properties, atomic force microscopy (AFM, Oxford instruments Asylum Research) to examine the surface morphology, and the electrical conductivity σ was measured at room temperature in a coplanar structure obtained with evaporation of four golden stripes on the deposited film surface; the measurements were performed with keithley Model 2400 Low Voltage Source Meter instrument.

3. Results and discussion

The XRD spectra recorded in different films are shown in Fig. 2. in the case of the In_2O_3/ITO films, The XRD pattern shows only two reflection peaks at 30.59° and 51.15° assigned to (222) and (440) planes. However, The XRD pattern obtained for the In_2O_3/Si films shows several reflection peaks located at 21.61°, 30.34°, 35.65°, 51.16° and 60.73° corresponding to the (211), (222),(400),(440) and (622) crystallographic planes of In_2O_3 cubic structure, respectively (All peaks from XRD patterns coincide well with those given in the JCPDS data card (6–416)). In addition to the presence of Si peak at 69.42° (JCPDS 27–1402file). N. Tripathi et al. [13] also found that the number of diffraction peaks Increase for the In_2O_3 films deposited on the Si substrate. However, Liu et al. [14] observed that the growth direction of Indium oxide on GaAs ⟨111⟩ is limited by the orientation of the substrate. On the other hand, in the case of In_2O_3/Si films the intensity ratio I(400)/I(222) is about 0.33. For In_2O_3 powders the last ratio is ~0.3. This shows randomly oriented growth on Si substrate. However, In_2O_3/ITO films possess a strong crystallographic texture along the

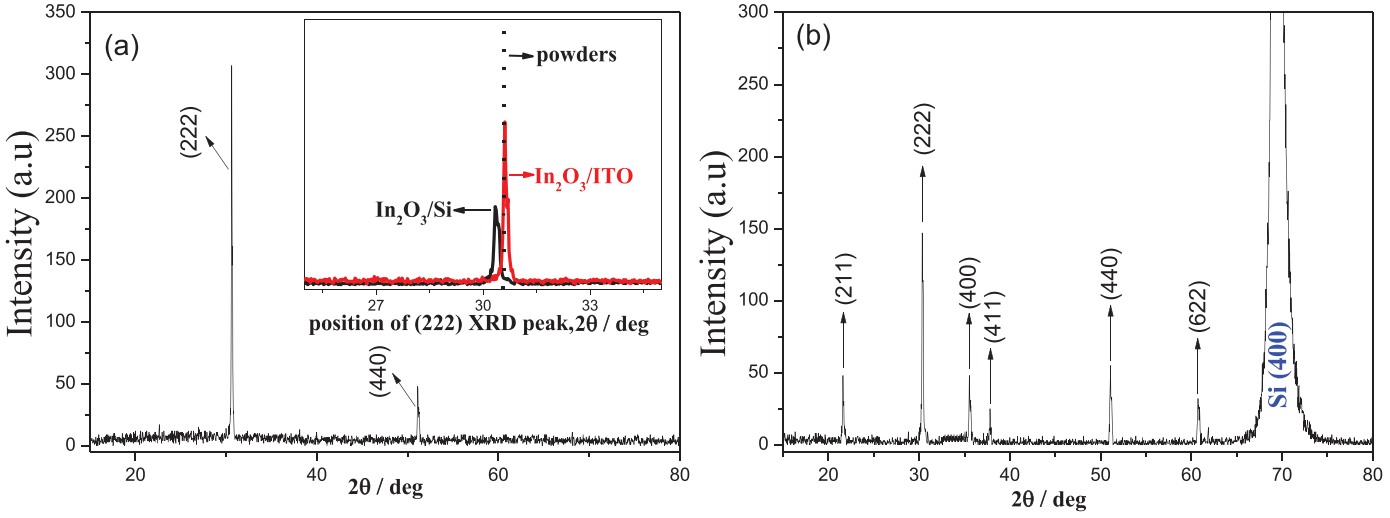

Fig. 2. XRD patterns of In_2O_3/ ITO (a) and In_2O_3/Si (b) thin films.

Table 2
Evaluated data of indium oxide films deposited on ITO and Si single crystal substrate.

Substrates	lattice mismatch (Δa)	Crystallite size (nm)	Lattice constant (Å)	Strain (ϵ) * 10^{-3}	Dislocationdensity (δ) × 10^{14} lines/m^2
ITO coated glass	0.01	66.5	10.11	0.39	2.26
Si single crystal	0.88	18	10.18	2.84	30.8

(222) plane, which indicates that the crystalline state of these layers has improved. This can be attributed to the lattice mismatch between In_2O_3 films and the used substrates. The lattice constant of the conducting glass substrate (ITO) matches with the lattice constant of the deposited films. Therefore, the In_2O_3 film grows in perfect registry with the conducting glass substrate. However, for the In_2O_3/Si films, the lattice constant of the single crystalline Si substrate is smaller than the lattice of the deposited films leading to create large densities of defects in the interface film-substrate wish propagate into the In_2O_3 film and consequently, the increasing of the structural disorder of In_2O_3/Si films. The calculated values of the lattice mismatch between the deposited films and the used substrates confirm this explanation (see Table. 2). On the other hand, the low crystalline state of the In_2O_3/Si films may originate from the difference of crystalline structural between the deposited film and the Si substrate [15]. Also, it is interesting to note that the XRD spectrum of the In_2O_3/Si films shows a shift towards lower angle for the intense In_2O_3 (2 2 2) peak (see the Fig. 2 (inset)). This indicates a lattice expansion [9,16].

The average grain size (D), strain (ϵ), lattice mismatch (Δa), lattice constant (a) and the dislocation density (δ) of the films from the preferred orientation (222) plane are estimated using following equations [9,17]:

$$D = \frac{0.9\lambda}{\beta \cos\theta} \quad (1)$$

$$\epsilon = \beta \cos(\theta)/4 \quad (2)$$

$$a = d(H^2 + K^2 + L^2)^{1/2} \quad (3)$$

$$\Delta a = \left(a_{In_2O_3} - - a_{substrate}\right)/ a_{In_2O_3} \quad (4)$$

$$\delta = 1/D^2 \quad (5)$$

where D is the crystallite size, ε is the strain, a is the lattice constant, θ is the Bragg's angle, β is the full width at half maximum (FWHM) of the (222) peak, λ is the X-ray wavelength, and (h, k, l) are the Miller indices; and (d) is the interplanar distance. The calculated values are listed in the Table 2. It is found that the grain size increase for the In_2O_3/ITO films (66.5 nm). However, their value decrease considerably in the case of the In_2O_3/Si films (18 nm). This may originate from the retarded crystal growth for the In_2O_3/Si films. Due to the high value of the lattice mismatch (0.88) between In_2O_3 and Si, the densities of defects in the interface film-substrate increase which leads to the stretched lattice (a = 10.18 nm) that can increase the lattice energy and diminish the driving force of growth. The dislocation density decrease for the In_2O_3/ITO films (2.26 × 10^{14} lines/m^2). This is due to the improvement of crystalline quality of these films.

In Fig. 3, we have reported the AFM images of In_2O_3/ITO (Fig. 3.a) and In_2O_3/Si films (Fig. 3.b). It can be observed that the In_2O_3/ITO films exhibit a smooth surface (Fig. 3a) however the In_2O_3/Si films show a rough surface (Fig. 3b). This difference in surface aspect, could be originate from the change in the growth mode of the films. In the case of the films deposited on the ITO substrate, the lattice mismatch is very small (lattice mismatche $^<$ 2%). the deposited films grows in the two dimensional (2D) layer-by-layer mode (Frank–van der Merwe Mode). however, In the case of the films deposited on the Si substrate, the growth mechanism is controlled by the 3D island growth mode (Volmer–Weber mode) due to the higher lattice mismatch [18,19]. the surface roughness (RMS) of the In_2O_3/ITO films is 9.83 nm while the RMS roughness obtained for the In_2O_3/Si films is 36.34 nm. Increase of the RMS roughness may be due to the transformation of layer-by layer (2D) growth into island (3D) growth [20,21].

In Fig. 4 we have drawn the variation of the deposition rate for the In_2O_3/ITO and In_2O_3/Si films. The deposition rate is estimated from the ratio of film thickness on the deposition time fixed at 4 min. As can be seen, The In_2O_3/ ITO films showed a higher value of deposition rate (film thickness) than the In_2O_3/Si films. We speculate that decrease of the deposition rate (film thickness) in the case of the In_2O_3/Si films may originate from the high value of the lattice mismatch (0.88), the later diminish the driving force of the growth and consequently, the deposition rate (film thickness) decrease. In addition, this difference in the deposition rate (film thickness) probably due to the high nucleation rate at the beginning formation of In_2O_3/Si films; the nucleation rate is faster than the deposition rate of the In_2O_3/Si films. It is well know that the preferred nucleation in the initial stage of films formation leads to the increase in the deposition rate of the films. Increase of the number diffraction peaks for the In_2O_3/Si films supports this explanation (see the Fig. 4 (inset)).

Additional information on the structure of In_2O_3/ITO and In_2O_3/Si films was obtained by Raman spectroscopy. Fig. 5 shows the Raman spectra of the deposited films. Group theory predicts the Raman modes for bcc-In_2O_3, such as 4Ag (Raman), 4Eg (Raman), 14Tg (Raman), 5Au (inactive), and 16Tu (infrared) modes [22]. The In_2O_3/ITO spectrum (Fig. 5.a) shows several peaks located at 132, 306, 361 and 630 cm^{-1}. These peaks are assigned to vibrational modes of the deposited indium oxide films, such as: the bending (δ)-vibration of InO_6 for the peak located at 306 cm^{-1} and In–O–In stretching vibrations modes for the peak located at 361 cm^{-1} [23,24]. However, the In_2O_3/Si spectrum (Fig. 5.b) shows two vibrational modes at 136 and 310 cm^{-1}. The vibrational modes observed for both films correspond to bcc-In_2O_3, agreeing well with the previous reported results [13,25]. Moreover, a small line width of Raman spectrum for the In_2O_3/ITO films indicates that these films have a very good crystal quality than the In_2O_3/Si films [25], as already indicated by the XRD analysis. On the other hand, it is clear that the position of the peaks for the In_2O_3/Si films is shifted. This is due to the increase of the strain in the crystallite (ϵ = 2.84 10 $^{-3}$) [26].

The most import feature in the Raman analysis is the decrease of the number vibrational modes for the In_2O_3/Si films. This is due to the high structural disorder of these films; the structural disorder destroys the long range coherence of phonons and consequently, the breaking of the Raman selection rules [27]. Increase of the structural disorder for the In_2O_3/Si films explained in the XRD analysis.

The In_2O_3/ITO film showed higher value of conductivity (σ = 5 × 10^2 $\Omega^{-1}cm^{-1}$) than the In_2O_3/Si film. The decrease in conductivity for In_2O_3/Si film (σ = 10^2 $\Omega^{-1}cm^{-1}$) may be explained on the basis of film crystallinity because the In_2O_3/ITO and In_2O_3/Si films show an appreciable difference in the crystallites size (ΔG = 48.5 nm). The small grain size for the In_2O_3/Si films (G = 18 nm) leads to an increase of scattering and trapping centers in the grain boundary and thus a decrease in conductivity [8,28,29]. The same opinion is held by R.K. Gupta et al. [30] who found that the electrical resistivity of IMO thin films decreases due to improvement in the film crystallinity at higher temperatures. In addition, Z. Yuan et al. [31] found that the grain boundary scattering is possibly the dominant scattering mechanism limiting the mobilities of In_2O_3 thin films. On the other hand, the low conductivity of the In_2O_3/Si film can be attributed

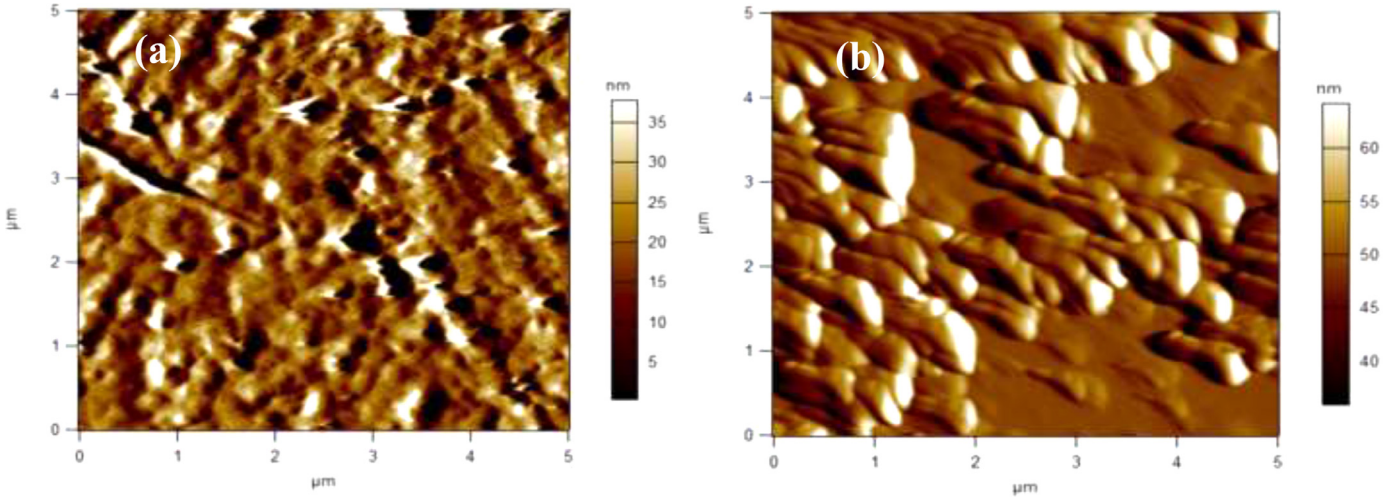

Fig. 3. The AFM images of (a) In_2O_3/ITO and (b) In_2O_3/Si films.

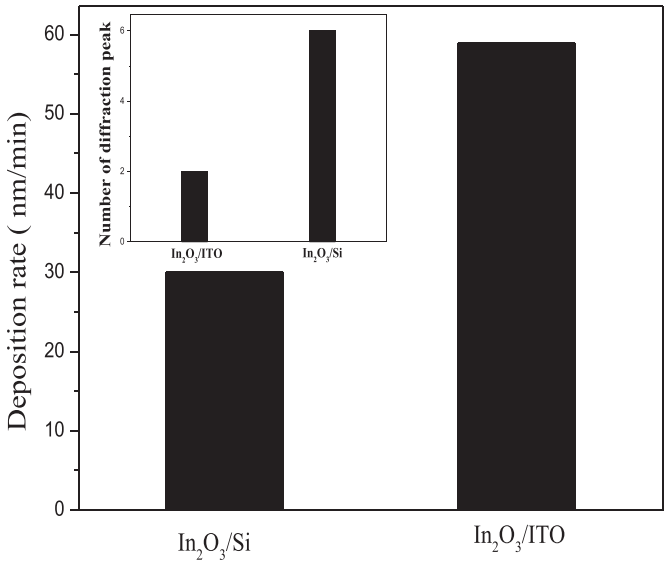

Fig. 4. Deposition rate of In_2O_3/ITO and In_2O_3/Si films.

from the scattering of conductive electrons by film surface and interface between In_2O_3 and Si [32,33]. It is well know that the high dense and packed grains decrease the number of scattering centers and trapping centers in the grain boundaries and consequently, the increasing of the carrier mobility and electron concentration [34], and the surface morphology of the In_2O_3/ITO films supports this explanation. On the other hand, increase of the conductivity for the In_2O_3/ITO films is probably due to the decrease in the dislocation density in this film [35].

4. Conclusion

In the present paper, we have investigated In_2O_3 thin films prepared on ITO coated glass and Si single crystal substrates by ultrasonic spray method. We found that the structural and electrical properties of In_2O_3 thin films were strongly affected by substrate. The In_2O_3/ITO films are polycrystalline with a preferred grain orientation along the (222) plane. However, films deposited on Si single crystal substrate, exhibit randomly oriented growth. The result of Raman analysis provided the information regarding the improved crystallinity and structure of In_2O_3 in ITO coated glass substrate. AFM images reveal that the film on each substrate realizes a different topography. For the ITO substrate, the deposited films grows in the two dimensional (2D) layer-by-layer mode (Frank–van der Merwe Mode), while on Si substrate, the growth mechanism is controlled by the 3D island growth mode. The film deposited

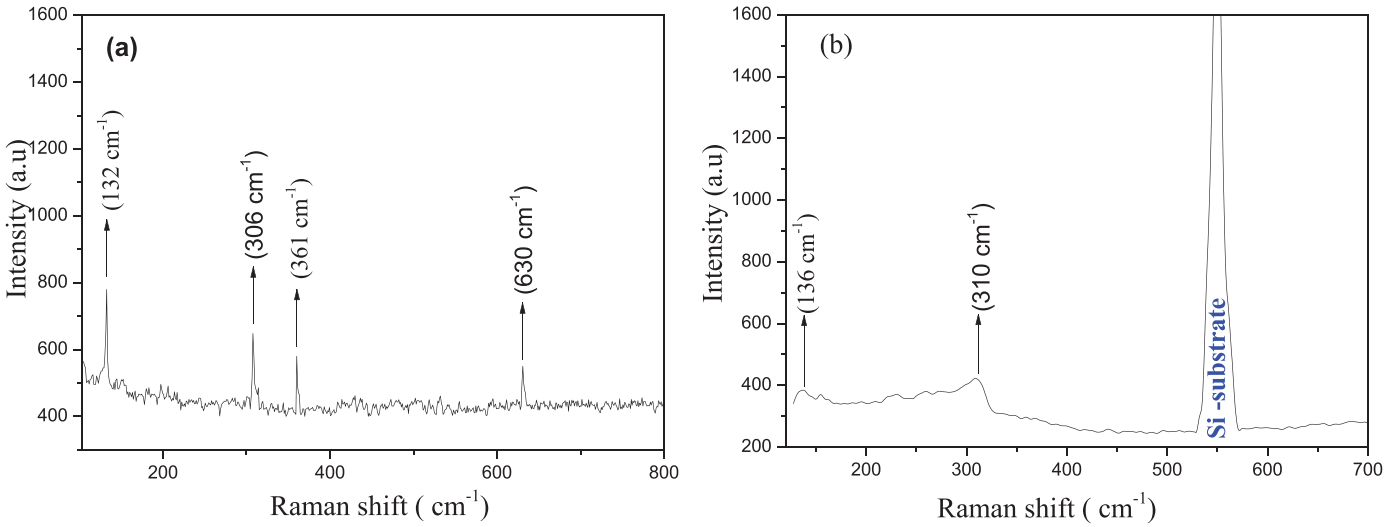

Fig. 5. The Raman spectra of In_2O_3/ITO (a) and In_2O_3/Si (b) films.

on ITO coated glass substrate is found to exhibit a higher value of conductivity ($\sigma = 5 \times 10^2\ \Omega^{-1}cm^{-1}$) than the In_2O_3/Si films.

Declaration of Competing Interests

None.

Supplementary materials

Supplementary material associated with this article can be found, in the online version, at doi:10.1016/j.surfin.2020.100579.

References

[1] M. Girtan, H. Cachet, et al. Thin Solid Films 427 (2003) 406.
[2] Z. Kaiyu, J. Wang, Thin Solid Films 162 (1988) 305.
[3] L.M. Wang, et al. J. Phys. Chem. Solids 69 (2008) 527–530.
[4] A. Subrahmanyam, U.K. Barik, J. Phys. Chem. Solids 67 (2006) 1518–1523.
[5] S. Parthiban, V. Gokulakrishnan, E. Elangovan, Thin Solid Films 524 (2012) 268–271.
[6] A. Bourlange, D. Payne, R. Jacobs, R. Egdell, J. Foord, A. Schertel, P. Dobson, J. Hutchison, Chem. Mater. 20 (2008) 4551–4553.
[7] J. Phys. Chem. Solids 68 (2007) 1380–1389.
[8] A. Bouhdjer, A. Attaf, H. Saidi, H. Bendjedidi, Y. Benkhetta, I. Bouhaf, J. Semicond. 36 (8) (2015).
[9] A. Bouhdjer, A. Attaf, H. Saidi, Y. Benkhetta, M.S. Aida, I. Bouhaf, A. Rhil, Optik 127 (2016) 6329–6333.
[10] A. Bouhdjer, H. Saidi, A. Attaf, M.S. Aida, Mohamed JlassI, I. Bouhaf, Y. Benkhetta, H. Bendjedidi, Optik 127 (2016) 7319–7325.
[11] A. Attaf, A. Bouhdjer, H. Saidi, M.S. Aida, N. Attaf, H. Ezzaouia, Thin Solid Films 625 (2017) 177–179.
[12] L. Álvarez-Fraga, et al. Appl. Surf. Sci. 344 (2015) 217–222.
[13] N. Tripathi, et al. Appl. Surf. Sci. 256 (2010) 7091–7095.
[14] H.F. Liu, et al. J. Cryst. Growth 311 (2009) 268–271.
[15] J.-B. Lee, et al. Thin Solid Films 447 – 448 (2004) 296–301.
[16] Z. Qiao, R. Latz, D. Mergel, Thin Solid Films 466 (2004) 250–258.
[17] R.K. Gupta, et al. Appl. Surf. Sci. 255 (2009) 8926–8930.
[18] D.J. Eaglesham, M. Cerullo, Dislocation-free Stranski-Krastanow growth of Ge on Si (100), Phys. Rev. Lett. 64 (16) (1990) 1943–1946.
[19] Jasprit Singh, Electronic and Optoelectronic Properties of Semiconductor Structures, Cambridge University Press, 2003, p. 31.
[20] K. Murakami, K. Nakajima, S. Kaneko, Thin Solid Films 515 (2007) 8632.
[21] I. Oja Acik, et al. Appl. Surf. Sci. 256 (2009) 1391–1394.
[22] D. Liu, W.W. Lei, B. Zou, High pressure X-ray diffraction and Raman spectra study of indium oxide, J. Appl. Phys. 104 (2008) 083506–083511.
[23] M. Kaur, N. Jain, K. Sharma, S. Bhattacharya, M. Roy, A. Tyagi, S. Gupta, J. Yakhmi, Sens. Actuators B 133 (2008) 456–461.
[24] J. Gwamuri, M. Marikkannan, J. Mayandi, K.P. Bowen, M.P. Joshua, Materials 9 (2016) 63.
[25] O.M. Berengue, et al. J. Phys. D: Appl. Phys. 43 (2010) 045401.
[26] M. Lamri Zeggar, et al. Mater. Sci. Semicond. Process. 30 (2015) 645–650.
[27] Olivia M Berengue, Ariano D Rodrigues, Cleocir J Dalmaschio, Alexandre J C Lanfredi, Edson R Leite, Adenilson J Chiquito, J. Phys. D: Appl. Phys. 43 (2010) 045401(4pp).
[28] V.F. Korzo, V.N. Chernyaev, Phys. Stat. Sol. 20 (1973) 695.
[29] J. Bardeen, W. Shockley, Phys. Rev. 80 (1950) 72.
[30] R.K. Gupta, et al. Appl. Surf. Sci. 254 (2008) 4018–4023.
[31] Z. Yuan, et al. Thin Solid Films 519 (2011) 3254–3258.
[32] A.F. Mayadas, M. Shatzkes, Electrical-resistivity model for polycrystallinefilms: the case of arbitrary reflection at external surfaces, Phys Rev B 1 (1970) 1382- 9.
[33] C.-C. Yu, et al. Vacuum 102 (2014) 63–66.
[34] D. Song, P. Widenborg, W Chin, Solar Energy Mater. Solar Cells 73 (2002) 17.
[35] S. Parthiban, V. Gokulakrishnan, E. Elangovan, G. Gonçalves, K. Ramamurthi, E. Fortunato, R. Martins, Thin Solid Films 524 (2012) 268.